Peer-reviewed version available at Metals 2019, 9, 559; doi:10.3390/met9050559

Article

The dehydrogenation mechanism and reversibility of $LiBH_4$ doped by active Al* derived from AlH_3

Qing He [1,2], Dongdong Zhu [1,*], Xiaocheng Wu [2], Duo Dong [1], Xiaoying Jiang [1] and Meng Xu [1]

[1] Key Laboratory of Air-driven Equipment Technology of Zhejiang Province, Quzhou University, Quzhou 324000, China; helinqi@163.com (Q.H.); dongduohit@163.com (D.D.); qz_jxy1@163.com (X.J.); xmm2021@163.com (M.X.)

[2] Department of Materials Science and Engineering, Zhejiang University, Hangzhou 310058, China; 11026032@zju.edu.cn (X.W.)

* Correspondence: zhudd8@163.com; Tel.: +86-1356-700-5297

Abstract: A detailed analysis of the dehydrogenation mechanism and reversibility of $LiBH_4$ doped by active Al* derived from AlH_3 was performed by thermogravimetry (TG), differential scanning calorimetry (DSC), mass spectral analysis (MS), powder X-ray diffraction (XRD), scanning electronic microscopy (SEM) and Fourier transform infrared spectroscopy (FTIR). The results show that the dehydrogenation of $LiBH_4$/Al* is a five-step reaction: (1) $LiBH_4 + Al \rightarrow LiH + AlB_2 +$ "Li-Al-B-H" $+ B_2H_6 + H_2$; (2) the decomposition of "Li-Al-B-H" compounds liberating H_2; (3) $2LiBH_4 + Al \rightarrow 2LiH + AlB_2 + 3H_2$; (4) $LiBH_4 \rightarrow LiH + B + 3/2H_2$; (5) $LiH + Al \rightarrow LiAl + 1/2H_2$. And the reversibility of $LiBH_4$/Al* composite is based on equation as follows: $LiH + LiAl + AlB_2 + 7/2H_2 \leftrightarrow 2LiBH_4 + 2Al$. The extent of dehydrogenation reaction between $LiBH_4$ and Al* greatly depends on the precipitation and growth of reaction products (LiH, AlB_2 and LiAl, etc.) on the surface of Al*. A passivation shell of Al* formed by these products is the kinetic barrier to the dehydrogenation of $LiBH_4$/Al* composite.

Keywords: $LiBH_4$; Al; dehydrogenation mechanism; kinetic properties; reversibility

1. Introduction

Hydrogen is recognized as an ideal energy vector with the advantages of high combustion value and zero pollution [1-3]. However, the storage of hydrogen is still challenging for its on-board application. Hydrogen energy can be stored in gas, liquid and solid forms, among which solid hydrogen storage is the safest. Currently, complex metal hydrides are considered as the most promising hydrogen storage materials due to their large hydrogen storage capacities [4-6].

Lithium borohydride ($LiBH_4$) has drawn much attention for on-board hydrogen storage due to its theoretical hydrogen storage capacity as high as 18.5wt.%, which far exceed the requirement of vehicle hydrogen storage material by the US department of energy [7,8]. Unfortunately, $LiBH_4$ is thermodynamically stable and the dehydrogenation is only initiated when temperature is above 400 ℃ under 1 bar H_2. The reversibility of $LiBH_4$ is poor and the rehydrogenation requires a temperature over 600℃ under 155bar H_2 [9,10]. Various methods have been developed to improve the dehydrogenation properties and reversibility of $LiBH_4$. Some researchers [11-13] found that thermodynamic destabilization of $LiBH_4$ could be achieved by adding reactive hydride composites (RHC) to change the dehydrogenation steps of it. For instance, Vajo et al [9]. reported that the dehydrogenation reaction enthalpy was much lower than that of the pure $LiBH_4$ by doping with MgH_2. The formation of MgB_2 during dehydrogenation reaction destabilized $LiBH_4$ and the reversibility of $LiBH_4$-MgH_2 composite was also better than pure $LiBH_4$. After that, many metal hydrides or complex hydrides have been employed to improve the hydrogen storage properties of $LiBH_4$ [14-22].

The metallic activity of Al and Mg is close. According to the theoretical calculation based on phase diagram, the decomposition temperature of $LiBH_4$/Al composite was predicated to be

Peer-reviewed version available at Metals 2019, 9, 559; doi:10.3390/met9050559

significantly lower than that of pure $LiBH_4$ [23]. So Al has been popularly employed as another destabilization agent to improve the hydrogen desorption properties of $LiBH_4$. The Al source can be either a metallic Al or a complex hydrides containing Al [24-26]. However, the metallic Al is usually coated with an oxide layer, which greatly limits the improvement of dehydrogenation and reversibility of $LiBH_4$. And the utilization of Al-containing hydrides will inevitably introduce the influence of other atoms on the de/rehydrogenation reaction. In order to investigate the mechanism and influence of pure Al on the dehydrogenation and reversibility of $LiBH_4$, an as-prepared Al (denoted Al*) derived from AlH_3 was employed as destabilization agent. The hydrogen desorption properties and mechanism of $LiBH_4$/Al* composite were studied systematically, along with kinetic investigations using a Sievert-type apparatus. Kissinger method was used to calculate the activation energy of the main dehydrogenation step of $LiBH_4$/Al* composite and its reversibility was also discussed.

2. Materials and Methods

The $LiBH_4$ powder (95% purity; Acros Organics) and Al powder (99% purity; Sinopharm Group) were employed as raw materials. AlH_3 was synthesized as follows: $LiAlH_4$ and $AlCl_3$ were dissolved in diethyl ether at a molar ratio of 3:1. After a period of reaction based on equation (1), the precipitate LiCl was filtered off and the filtrate containing AlH_3 was separated from mixture. The pure AlH_3 was then obtained from the filtrate by dried and de-ethers in vacuum. Finally, AlH_3 was completely dehydrogenated to obtain active Al* by heating to 200℃ and holding for 2.5h. The dehydrogenation curves of AlH_3 and XRD patterns of AlH_3 before and after dehydrogenation are shown in Figure 1(a) and 1(b), respectively.

$$3LiAlH_4 + AlCl_3 \rightarrow 4AlH_3 + 3LiCl\downarrow \quad (1)$$

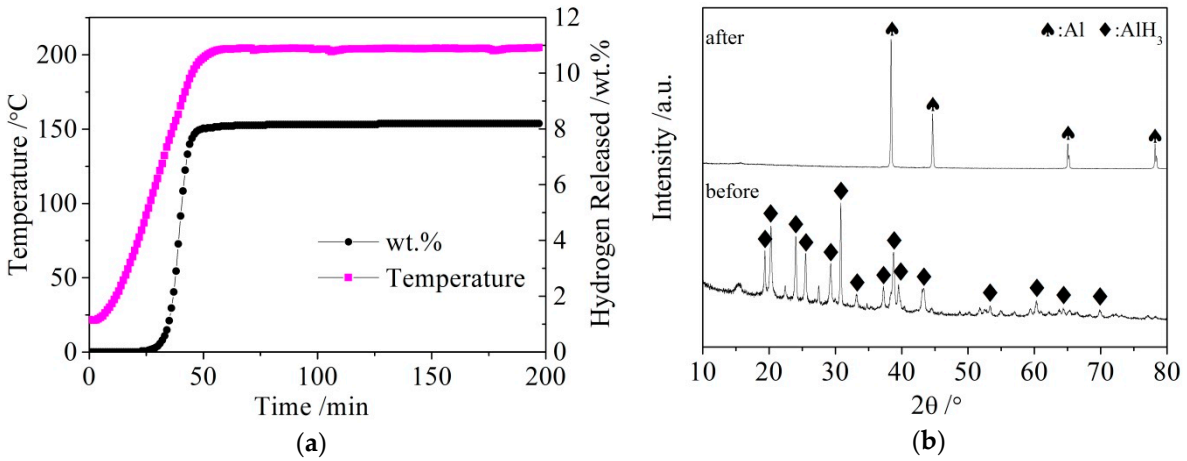

Figure 1. The dehydrogenation curves (**a**) of AlH_3 and XRD patterns (**b**) of AlH_3 before and after dehydrogenation.

The commercial Al powder was used for comparison with the as-prepared Al* in this study. The $LiBH_4$/Al and $LiBH_4$/Al* composites were synthesized by ball-milling using a QM-3SP4 planetary ball mill (Nanjing Nanda Instrument Plant). The ball to powder ratio was 45:1. The milling process was carried out at 400 rpm for 30 min under a 0.1 MPa argon atmosphere. To prevent the temperature from rising too fast during long-term milling, the milling process was paused every 6 min for cooling. All of the samples were handled in a Mikrouna glove box filled with high purity argon (99.999%) and controlled H_2O (<0.5 ppm) and O_2 (<0.1 ppm) concentrations for preventing contamination.

The morphologies of the as-received Al and as-prepared Al* were observed by a field emission scanning electronic microscopy (SEM, Hitachi S4800). The characterization of hydrogen desorption properties of the $LiBH_4$/Al and $LiBH_4$/Al* samples was carried out on a Sieverts-type apparatus [27]. The thermal events during dehydrogenation of the samples were investigated by thermogravimetry

/differential scanning calorimeter (TG/DSC, Netzsch STA449F3). For the isothermal hydrogen desorption measurements, the samples were rapidly heated to a set temperature (i.e., 100℃, 350℃, 500℃ and 600℃) and held for 3h under flowing argon of 50 ml/min. For the non-isothermal dehydrogenation (i.e., the temperature programmed desorption, TPD) measurements, the samples were heated gradually from room temperature to 600℃with a heating rate of 5℃/min. The hydrogen desorption spectra were collected synchronously using a mass spectrometer (MS, Netzsch QMS403C). The phase of the as-prepared samples and the dehydrogenation product of them at various temperatures were identified by X-ray diffraction technique (XRD, X'Pert Pro, Cu-Kα) and fourier transform infrared spectroscopy (FTIR, Beuker-Vector22). During XRD measurements, the samples were sealed with a polypropylene membrane to avoid exposure to any moisture or oxygen.

3. Results and Discussion

3.1. Dehydrogenation mechanism of the $LiBH_4$/Al composite*

The SEM images of the as-received Al particles and as-prepared Al* particles are shown in Figure 2. It can be seen that the particle size of the as-received Al is about 100 μm, while the particle size of active Al* derived from AlH_3 is only 1% of it. A sharp reduction in the particle size means a significant increase in the specific surface area.

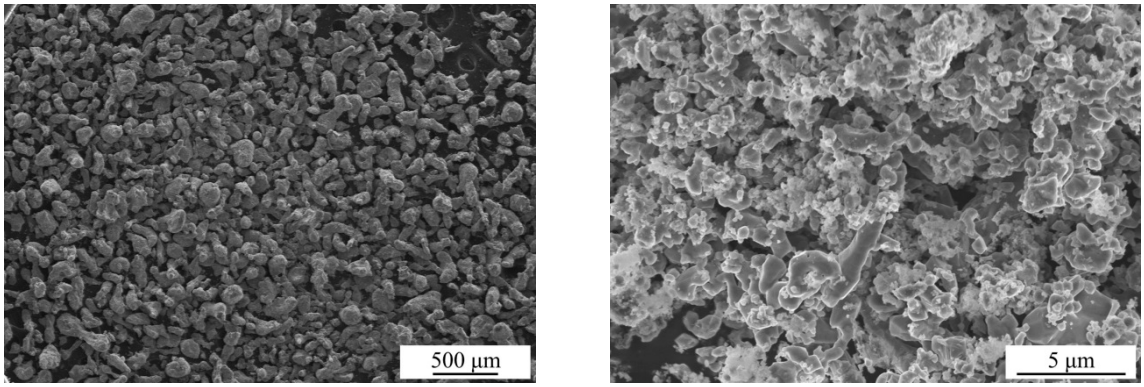

(**a**) (**b**)

Figure 2. SEM images of the as-received Al particles (**a**) and as-prepared Al* particles (**b**).

Figure 3 presents different simultaneous signals for the dehydrogenation of $LiBH_4$/Al and $LiBH_4$/Al* samples: the thermogravimetry (TG) signal, DSC signal and hydrogen signal plotted over the temperature. It can be seen from Figure 3a that the dehydrogenation curves of $LiBH_4$/Al and $LiBH_4$/Al* composites are almost the same before 350℃, and they both liberate about 0.1 wt.% of H_2. After being heated to 350℃, the dehydrogenation rate of $LiBH_4$/Al* is obviously faster than that of $LiBH_4$/Al. Finally, the total dehydrogenation amount of $LiBH_4$/Al and $LiBH_4$/Al* samples at 600℃ reached 5.5 wt.% and 6.2 wt.%, respectively. It can be ascribed to the Al* derived from AlH_3 has larger specific surface area, and the oxide-free surface of Al* possess higher chemical reactivity. So that the dehydrogenation reaction of $LiBH_4$/Al* is more sufficient than $LiBH_4$/Al.

The DSC/MS curves of $LiBH_4$, $LiBH_4$/Al and $LiBH_4$/Al* were displayed in Figure 3b, 3c and 3d, respectively. The endothermic peak in the DSC curve of pure $LiBH_4$ (Figure 3b) at 112℃ corresponds to the crystal transformation from orthorhombic phase (*o*-$LiBH_4$) to hexagonal phase (*h*-$LiBH_4$), while the endothermic peak at 288℃ corresponds to the melting of *h*-$LiBH_4$ [28]. $LiBH_4$ is dehydrogenated in the temperature range of 400℃ to 550℃, in which the dehydrogenation rate reached the maximum around 481℃. So the endothermic peak at this temperature is ascribed to the decomposition of $LiBH_4$ based on equation (2).

$$LiBH_4 \rightarrow LiH + B + 3/2H_2 \uparrow \quad (2)$$

There are three endothermic peaks at 465℃, 482℃ and 530℃ in the DSC curve of $LiBH_4$/Al sample (Figure 3c). Each endothermic peak corresponds to a hydrogen evolution peak in the MS curve. The endothermic peak at 482℃ is in good agreement with that of the decomposition of $LiBH_4$ mentioned above. Compared with figure 3b, the new endothermic peaks at 465℃ and 530℃ should be related to the reaction of $LiBH_4$ and the added Al. According to the work of other researchers [29-31], the endothermic peak at 465℃ is ascribed to $LiBH_4$ reacts with Al forming LiH, AlB_2 and liberating H_2 (equation (3)), and the endothermic peak at 530℃ is attributed to the reaction of LiH with Al to form LiAl alloy and H_2 (equation (4)).

$$2LiBH_4 + Al \rightarrow 2LiH + AlB_2 + 3H_2 \uparrow \quad (3)$$

$$LiH + Al \rightarrow LiAl + 1/2H_2 \uparrow \quad (4)$$

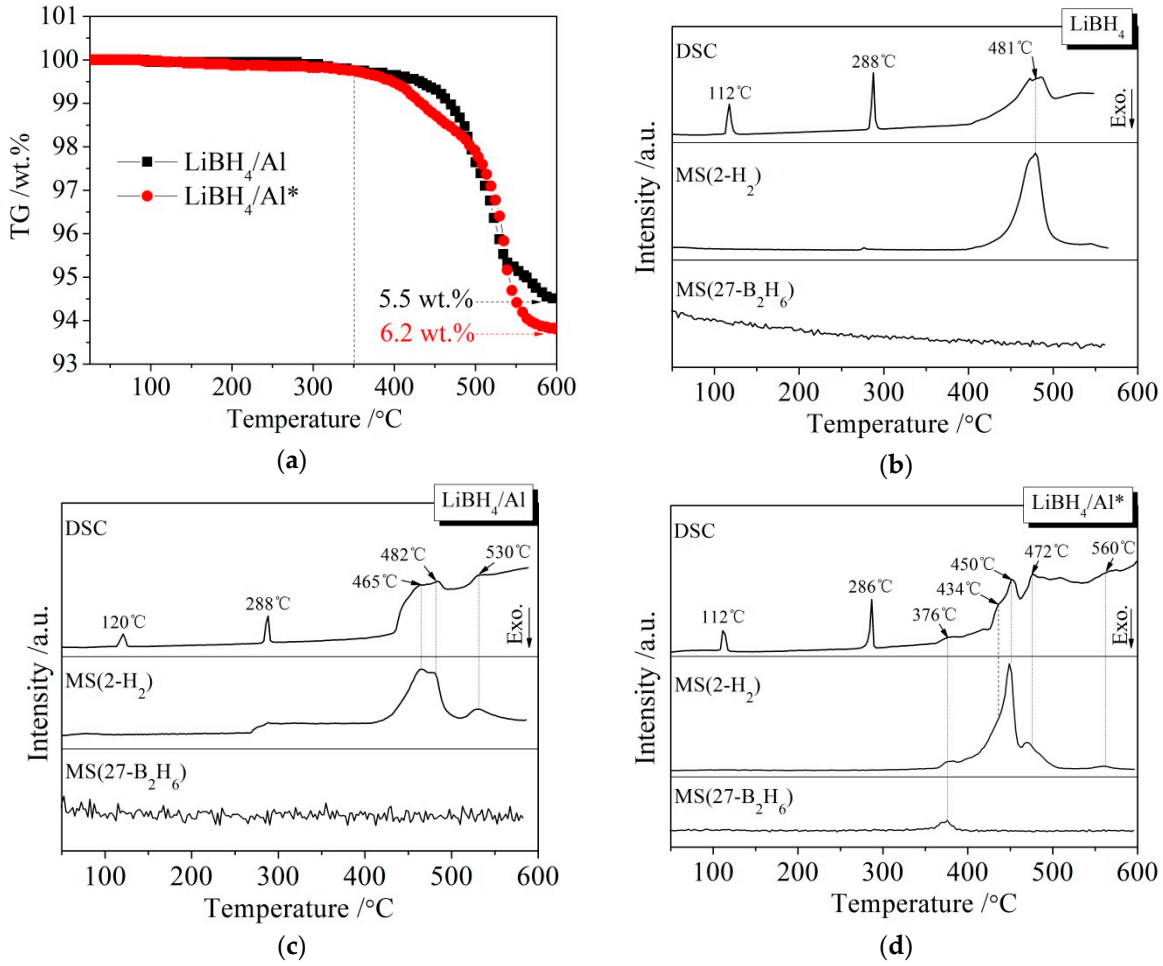

Figure 3. TG curves (**a**) of $LiBH_4$/Al and $LiBH_4$/Al* samples and DSC/MS curves of $LiBH_4$ (**b**), $LiBH_4$/Al (**c**) and $LiBH_4$/Al* (**d**) samples.

It can be seen from Figure 3d that the dehydrogenation behavior of $LiBH_4$/Al* is more sophisticated than that of $LiBH_4$/Al. There is a tiny endothermic peak appeared at 376℃ in the DSC curve of $LiBH_4$/Al* composite, accompanied by a small amount of H_2 and B_2H_6 desorption reflected in the MS curve. What's more, there are four endothermic peaks of dehydrogenation locate at 434℃, 450℃, 472℃ and 560℃. In order to investigate the mechanism of these thermal events, XRD and FTIR analyses were conducted on the solid products of $LiBH_4$/Al* sample at different dehydrogenation temperatures (e.g. 100℃, 350℃, 500℃ and 600℃). The results are shown in Figure 4 and Figure 5, respectively. It can be seen from Figure 4(a) that no new phase was detected when the sample was heated to 100℃. The shrinkage of the diffraction peaks of $LiBH_4$ is related to its crystal transformation. When the sample was heated to 350℃, some tiny diffraction peaks of AlB_2 and an unknown phase appeared. The unknown phase, marked "?", was also reported by

other researchers and considered to be compounds with components of Li-Al-B [32, 33]. Combined with the FTIR spectra in Figure 5(a), the diffraction peaks of LiH, overlapped with the diffraction peaks of Al, can also be found in Figure 4(a) at this stage. It indicates that $LiBH_4$ had started to react with Al* to form LiH, AlB_2 and compounds containing Li-Al-B. At the same time, B_2H_6 and H_2 were released and the rate reached a peak at 376℃ according to Fig. 3c. Therefore, the further decrease of the diffraction intensity of $LiBH_4$ at 350℃ (Figure 4(a)) can be attributed to its melting and hydrogen desorption reaction based on equation (5). In addition, AlB_2 is generally considered to be a product which makes the dehydrogenation system reversible, while B_2H_6 is a toxic gas which may be an problem for the future application of $LiBH_4$/Al* system.

$$LiBH_4 + Al \rightarrow LiH + AlB_2 + \text{“Li-Al-B”} + B_2H_6\uparrow + H_2\uparrow \quad (5)$$

When the sample was heated to 500℃, the $LiBH_4$ cannot be detected by the XRD analysis (Figure 4(a)) and the vibrational peaks of B-H stretching (2382 cm^{-1}, 2292 cm^{-1} and 2224 cm^{-1}) and bending (1125 cm^{-1}) disappeared (Figure 5(a)), indicating that $LiBH_4$ had been completely consumed in dehydrogenation reaction around 376℃, 434℃, 450℃ and 472℃ (Figure 3(d)). What's more, the diffraction peaks of LiAl appeared and the diffraction intensity of LiH and AlB_2 slightly inceased, while the peaks of Al weakened and the peaks of unknown components disappeared. Combined with the analyses of $LiBH_4$ and $LiBH_4$/Al samples, it can be reasonably assumed that the main dehydrogenation peak of $LiBH_4$/Al* around 450℃ (Figure 3(d)) is attributed to the reaction of $LiBH_4$ and Al to form LiH, AlB_2 and H_2 based on equation (3). The reaction temperature is lower than that of $LiBH_4$/Al sample probably because the higher chemical reactivity of Al* reduced the activation energy of the reaction. The dehydrogenation peak around 472℃ is ascribed to the self-decomposition of $LiBH_4$ forming LiH, B and H_2 based on equation (2). However, the diffraction peaks of B are not found in the XRD examination due to that B is in an amorphous state. Then the dehydrogenation peak around 434℃ is probably related to the decomposition of the unknown phase, which is deduced to be an complex hydride containing Li-Al-B. Therefore, the equation (5) can be modified to equation (6), where the unknown phase was denoted as “Li-Al-B-H”. Finally, the appearance of LiAl indicates that LiH had begun to react with Al* to form LiAl and liberate H_2 (equation (4)) before 500℃.

$$LiBH_4 + Al \rightarrow LiH + AlB_2 + \text{“Li-Al-B-H”} + B_2H_6\uparrow + H_2\uparrow \quad (6)$$

Compared with the XRD patterns at 500℃, no new phase was detected when the $LiBH_4$/Al* sample was heated to 600℃. The increase of the relative diffraction intensity of LiAl implies that the reaction of LiH with Al* continued from 500℃ to 600℃. The dehydrogenation rate of this reaction reached a peak at 560℃ according to Figure 3(d). The existence of LiH and Al suggests that the $LiBH_4$/Al* system still dehydrogenated incompletely even at 600℃. In fact, the actual dehydrogenation amount of $LiBH_4$/Al* sample is only 86.11% of the theoretical value (7.2 wt.%) according to Figure 3(a), indicating that there exists some kinetic barriers in the dehydrogenation reaction of $LiBH_4$/Al* composite.

The whole hydrogen desorption process of the $LiBH_4$/Al* sample, which is schematically shown in Figure 6, can be concluded as follows: As heating in the crucible, $LiBH_4$ first transformed from orthorhombic phase (o-$LiBH_4$) to hexagonal phase (h-$LiBH_4$) at 112℃ and melted at 288℃. Then the molten $LiBH_4$ reacted with Al* to form LiH, AlB_2 and "Li-Al-B-H" compounds while releasing B_2H_6 and H_2 based on equation (6) around 376℃. With the nucleation and growth of LiH, AlB_2 and "Li-Al-B-H" compounds on the surface of Al*, the reaction stopped when Al* was completely wrapped by these reaction products to form a passivation shell. When the temperature rose to 434℃, the decomposition of "Li-Al-B-H" compounds liberated a certain amount of H_2 and the encapsulated Al* exposed some new surfaces. So the main dehydrogenation reaction of $LiBH_4$ and Al* occurred around 450℃ to form LiH, AlB_2 and H_2 based on equation (3). Similarly, the reaction stopped when the surface of Al* was completely wrapped by LiH and AlB_2. Therefore, the excess molten $LiBH_4$ underwent self-decomposition to form LiH, B and H_2 (equation (2)) around 472℃. Boron (B) are not detected in the XRD examination because it is in an amorphous state. Finally, the product LiH reacted with Al* to form LiAl alloy and H_2 based on equation (4) when the

Preprints (www.preprints.org) | NOT PEER-REVIEWED | Posted: 15 April 2019 doi:10.20944/preprints201904.0158.v1

Peer-reviewed version available at Metals 2019, 9, 559; doi:10.3390/met9050559

sample was heated to 560℃. The actual dehydrogenation amount of $LiBH_4$/Al* sample did not reach the theoretical value since there were still non-contact and unreacted LiH and Al* at 600℃.

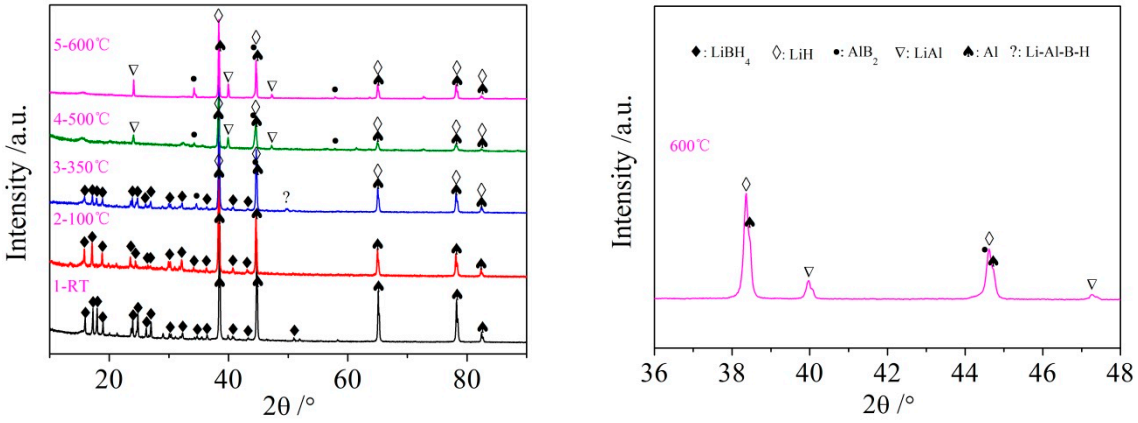

Figure 4. XRD patterns (**a**) of the $LiBH_4$/Al* sample obtained at different temperatures (room temperature, 100, 350, 500 and 600℃) and expanded XRD pattern of $LiBH_4$/Al* sample of 600℃ at 2θ range of 36-48°.

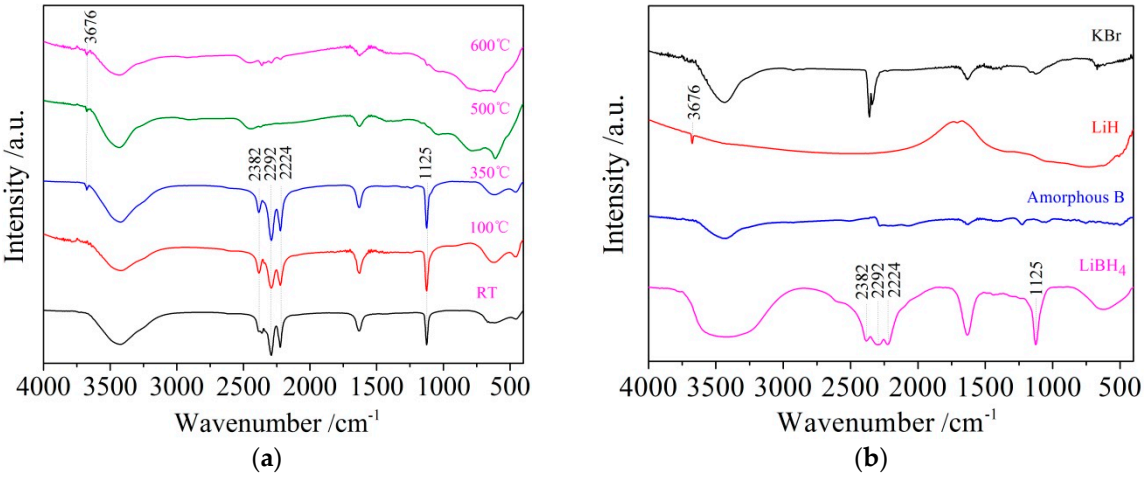

Figure 5. FTIR patterns of the $LiBH_4$/Al* sample (**a**) obtained at different temperatures (room temperature, 100, 350, 500 and 600℃) and reference substances (**b**) include KBr, LiH, amorphous B, and $LiBH_4$.

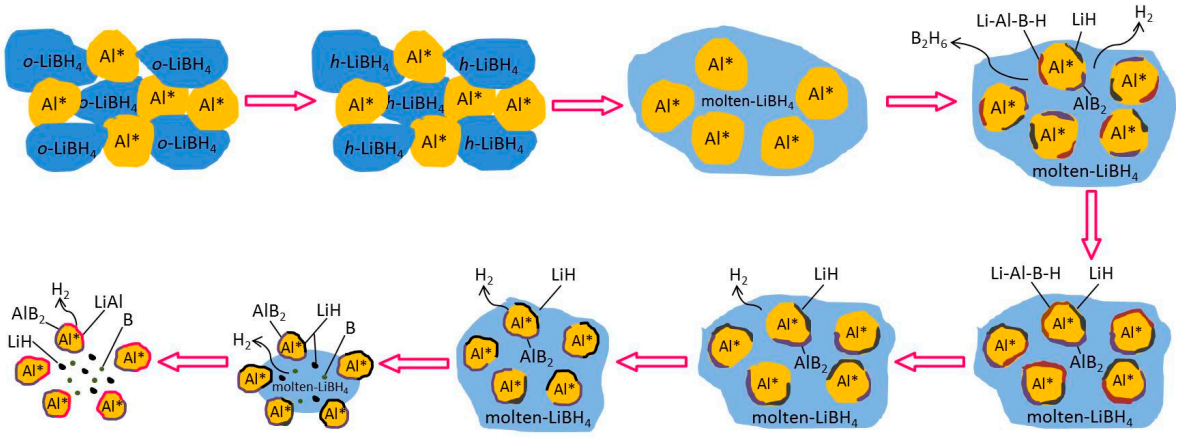

Figure 6. Schematic diagram of the dehydrogenation process of the $LiBH_4$/Al* sample.

3.2. Kinetic properties of the dehydrogenation of $LiBH_4$/Al composite*

The kinetic properties of the dehydrogenation of $LiBH_4/Al^*$ composite was studied using the Kissinger method, which assuming that the apparent activation energy (E_a) of dehydrogenation reaction is determined by equation (7).

$$\ln(\beta/T_m^2) = - E_a/RT_m + C \quad (7)$$

In this equation, β is the heating rate in thermal analysis and T_m represents the absolute temperature at the maximum reaction rate. Besides, R is the universal gas constant and C also represents a constant. Therefore, the E_a of the dehydrogenation reaction of $LiBH_4/Al^*$ composite can be obtained from the slope of a linearly fitted line in the $\ln(\beta/T_m^2)$-T_m^{-1} spectrum.

During the kinetic investigations, the $LiBH_4/Al$ and $LiBH_4/Al^*$ samples were heated to 600℃ at the rates of 5℃/min, 10℃/min and 20℃/min, respectively. The MS curves at various heating rates and the Kissinger spectra reflecting the E_a of the main dehydrogenation reaction are shown in Figure 7. It can be seen that the temperatures for the maximum dehydrogenation rate of $LiBH_4/Al^*$ at the heating rates of 5℃/min, 10℃/min and 20℃/min are 449.9℃, 471.1℃ and 485.2℃, respectively. All lower than that of $LiBH_4/Al$ at the same heating rates. The E_a of the main dehydrogenation reaction of $LiBH_4/Al^*$ is calculated to be 163.8 kJ/mol, while that of $LiBH_4/Al$ is 243.5 kJ/mol. This is in good agreement with the previous analysis that the larger specific surface area and higher chemical reactivity of Al* can reduce the activation energy and improve the kinetic properties of the dehydrogenation reaction.

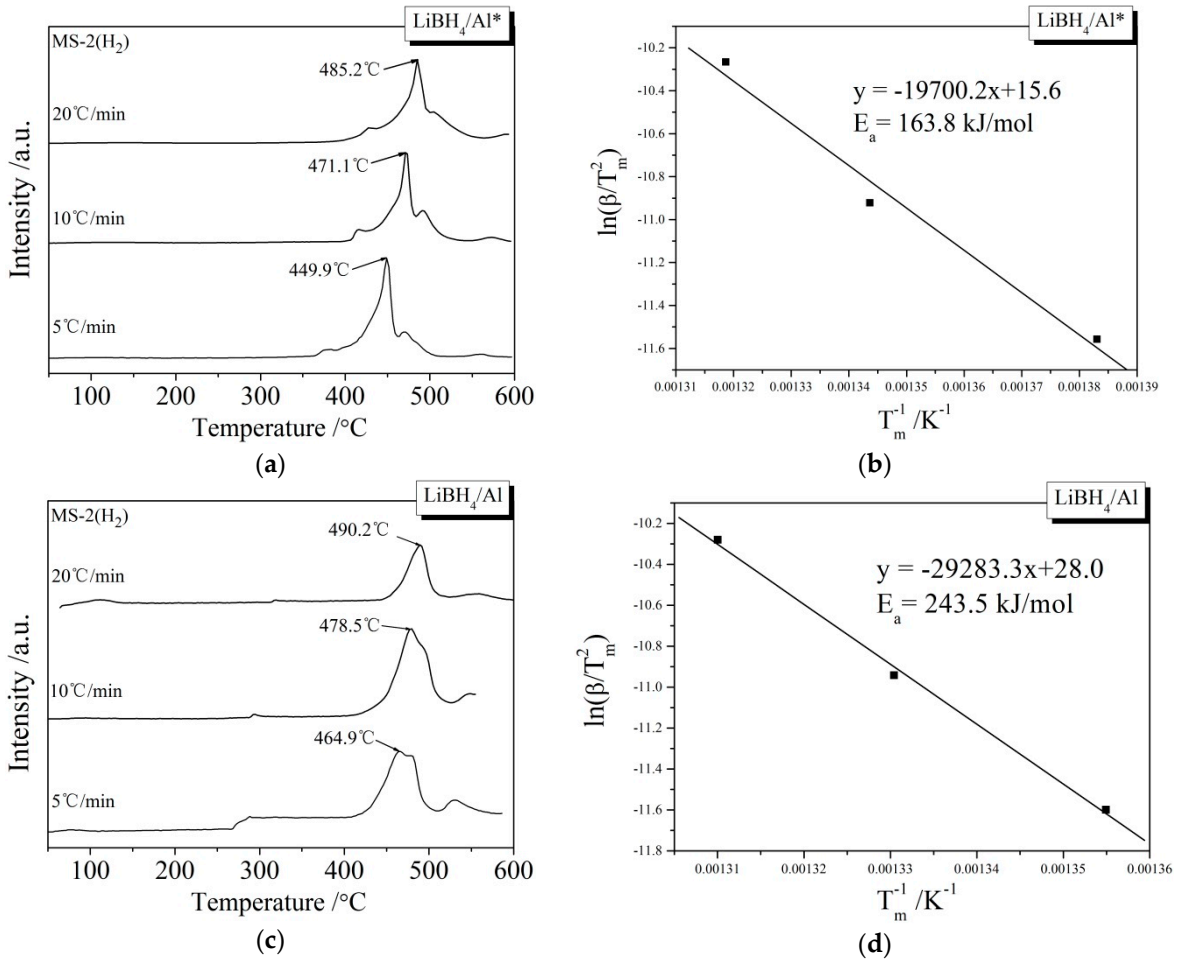

Figure 7. MS curves (**a**), (**c**) of $LiBH_4/Al^*$ and $LiBH_4/Al$ samples at different heating rates (5℃/min, 10℃/min and 20℃/min) and Kissinger spectra (**b**), (**d**) that $\ln(\beta/T_m^2)$ as a function of T_m^{-1} for the main dehydrogenation reaction of $LiBH_4/Al^*$ and $LiBH_4/Al$ samples.

3.3. Reversibility of the $LiBH_4/Al^*$ composite

In order to investigate the reversibility of $LiBH_4$/Al* composite, rehydrogenation test was carried out under 8 MPa H_2 at 400℃. The rehydrogenation curve of the sample is shown in Figure 8. It can be seen that the dehydrogenated $LiBH_4$/Al* sample quickly absorbed 0.8 wt.% of hydrogen within 2min at the beginning of test. And then it absorbed 2.6 wt.% of hydrogen in 60 min. After that, it entered the stable hydrogen absorption stage and reached saturation after 480 min. The total rehydrogenation capacity was 5.5 wt.%. Compared with the harsh rehydrogenation conditions reported by other researchers [10], the doping of active Al* derived from AlH_3 effectively improved the reversible hydrogen storage properties of $LiBH_4$.

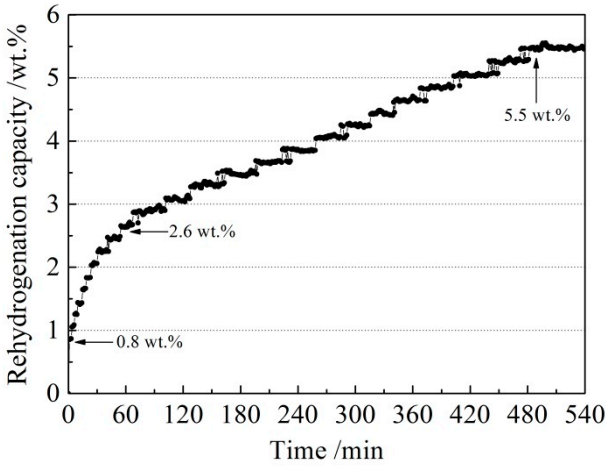

Figure 8. The rehydrogenation curve of dehydrogenated $LiBH_4$/Al* sample under 8 MPa H_2 at 400℃.

The rehydrogenation mechanism exploration was conducted using XRD and FTIR analysis on the rehydrided products of $LiBH_4$/Al* sample, and the results are shown in Fig. 9a and 9b, respectively. It can be seen from the XRD patterns that the diffraction peaks of LiAl, LiH and AlB_2 disappeared, while the diffraction peaks of $LiBH_4$ reappeared and the diffraction intensity of Al increased after rehydrogenation. Not to mention that the vibrational peaks of B-H stretching (2382 cm^{-1}, 2292 cm^{-1} and 2224 cm^{-1}) and bending (1125 cm^{-1}) were also detected in the FTIR spectra. Therefore, the reformation of $LiBH_4$ can be confirmed during the rehydrogenation process. Based on the above analysis, it can be safely concluded that the rehydrogenation process of $LiBH_4$/Al* is based on equation (8).

$$LiH + LiAl + AlB_2 + 7/2H_2 \leftrightarrow 2LiBH_4 + 2Al \quad (8)$$

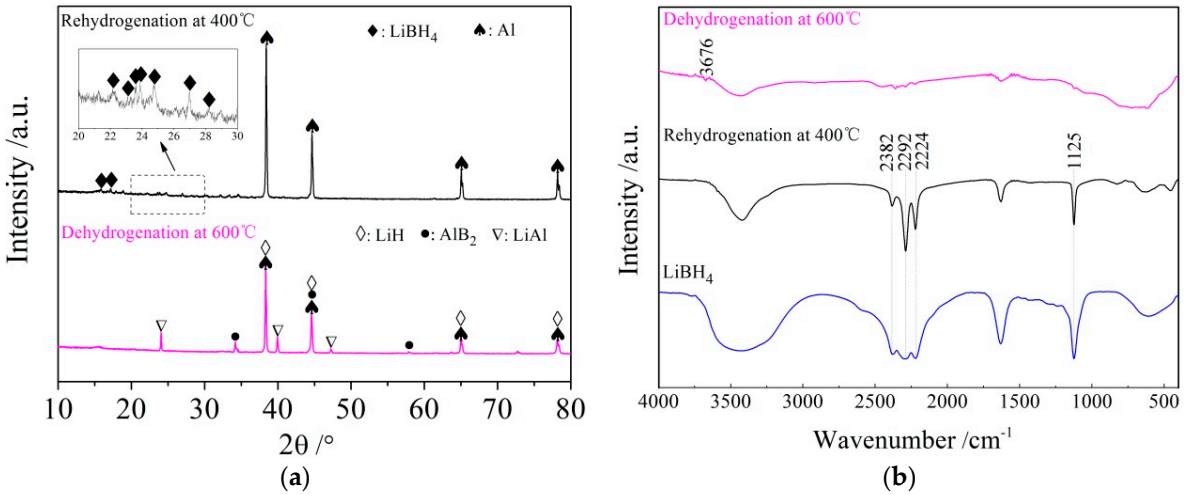

Figure 9. XRD patterns (**a**) and FTIR spectra (**b**) of $LiBH_4$/Al* sample before and after rehydrogenation.

4. Conclusions

The dehydrogenation of $LiBH_4$ doped by active Al* derived from AlH_3 has a five-step character: (1) $LiBH_4 + Al \rightarrow LiH + AlB_2 +$ "Li-Al-B-H" $+ B_2H_6 + H_2$; (2) the decomposition of "Li-Al-B-H" compounds liberating H_2; (3) $2LiBH_4 + Al \rightarrow 2LiH + AlB_2 + 3H_2$; (4) $LiBH_4 \rightarrow LiH + B + 3/2H_2$; (5) $LiH + Al \rightarrow LiAl + 1/2H_2$. And the reversibility of $LiBH_4$/Al* composite is based on equation as follows: $LiH + LiAl + AlB_2 + 7/2H_2 \leftrightarrow 2LiBH_4 + 2Al$.

The hydrogen desorption kinetics of $LiBH_4$ were effectively improved by doping with active Al* derived from AlH_3. Higher dehydrogenation capacity, lower activation energy and better reversibility of $LiBH_4$/Al* can be achieved due to the larger specific surface area and higher chemical reactivity of Al*. The extent of dehydrogenation reaction between $LiBH_4$ and Al* greatly depended on the precipitation and growth of reaction products (LiH, AlB_2 and LiAl, etc.) on the surface of Al*. A passivation shell of Al* formed by these products is the kinetic barrier to the dehydrogenation of $LiBH_4$/Al* composite. Therefore, next work should be focused on cracking the barrier to further improve the hydrogen storage properties of $LiBH_4$/Al* composite.

Author Contributions: Conceptualization, Q.H. and D.Z.; Methodology, Q.H. and D.D.; Data curation, M.X. and X.W.; Formal analysis, X.W.; Investigation, M.X. and X.J.; Resources, Q.H.; Supervision, Q.H.; Project administration, Q.H.; Funding acquisition, Q.H.; Writing-original draft preparation, X.W.; Writing-review and editing, Q.H. and D.Z.

Funding: This work was funded by the Zhejiang Provincial Natural Science Foundation of China (Grant Nos.LQ16E01002, Y18E010014), and the National Natural Science Foundation of China (Grant Nos. 51501100, 51801112, 51704001).

Conflicts of Interest: The authors declare no conflict of interest.

References

1. Parra D, Valverde L, Pino F J, et al. A review on the role, cost and value of hydrogen energy systems for deep decarbonisation. *Renewable and Sustainable Energy Reviews*, 2019, 101: 279-294.
2. Colbertaldo P, Agustin S B, Campanari S, et al. Impact of hydrogen energy storage on California electric power system: towards 100% renewable electricity. *International Journal of Hydrogen Energy*, 2019, 44(19): 9558-9576.
3. Zhao G, Nielsen E R, Troncoso E, et al. Life cycle cost analysis: A case study of hydrogen energy application on the Orkney Islands. *International Journal of Hydrogen Energy*, 2019, 44(19): 9517-9528.
4. Cuevas F. Introduction to complex metal hydrides. *Hydrogen Storage Materials*. Springer, Berlin, Heidelberg, 2018: 251-251.
5. Schneemann A, White J L, Kang S Y, et al. Nanostructured metal hydrides for hydrogen storage. *Chemical reviews*, 2018, 118(22): 10775-10839.
6. Rahnama A, Zepon G, Sridhar S. Machine learning based prediction of metal hydrides for hydrogen storage, part II: Prediction of material class. *International Journal of Hydrogen Energy*, 2019, 44(14): 7345-7353.
7. Wu R, Ren Z, Zhang X, et al. Nanosheet-like Lithium Borohydride Hydrate with 10 wt% of Hydrogen Release at 70° C as a Chemical Hydrogen Storage Candidate. *The journal of physical chemistry letters*, 2019, 10: 1872–1877.
8. DOE U S. Targets for onboard hydrogen storage systems for light-duty vehicles. *US Department of Energy, Office of Energy Efficiency and Renewable Energy and The FreedomCAR and Fuel Partnership*, 2009.
9. Vajo J J, Skeith S L, Mertens F. Reversible storage of hydrogen in destabilized $LiBH_4$. *The Journal of Physical Chemistry B*, 2005, 109(9): 3719-3722.
10. Matsuo M, Orimo S. Lithium Fast-Ionic Conduction in Complex Hydrides: Review and Prospects. *Advanced Energy Materials*, 2011, 1(2): 161-172.
11. Saldan I. A prospect for $LiBH_4$ as on-board hydrogen storage. *Central European Journal of Chemistry*, 2011, 9(5): 761-775.
12. Jepsen J, Capurso G, Puszkiel J, et al. Effect of the Process Parameters on the Energy Transfer during the Synthesis of the $2LiBH_4$-MgH_2 Reactive Hydride Composite for Hydrogen Storage. *Metals*, 2019, 9(3): 349.
13. Milanese C, Jensen T R, Hauback B C, et al. Complex hydrides for energy storage. *International Journal of Hydrogen Energy*, 2019, 44(15): 7860-7874.

14. Bösenberg U, Doppiu S, Mosegaard L, et al. Hydrogen sorption properties of MgH_2-$LiBH_4$ composites. *Acta Materialia*, 2007, 55(11): 3951-3958.
15. Puszkiel J A, Riglos M V C, Karimi F, et al. Changing the dehydrogenation pathway of $LiBH_4$-MgH_2 via nanosized lithiated TiO_2. *Physical Chemistry Chemical Physics*, 2017, 19(11): 7455-7460.
16. Mao J F, Guo Z P, Liu H K, et al. Reversible hydrogen storage in titanium-catalyzed $LiAlH_4$-$LiBH_4$ system. *Journal of Alloys and Compounds*, 2009, 487(1-2): 434-438.
17. Mao J, Guo Z, Leng H, et al. Reversible hydrogen storage in destabilized $LiAlH_4$-MgH_2-$LiBH_4$ ternary-hydride system doped with TiF_3. *The Journal of Physical Chemistry C*, 2010, 114(26): 11643-11649.
18. Noritake T, Aoki M, Towata S, et al. Crystal structure analysis of novel complex hydrides formed by the combination of $LiBH_4$ and $LiNH_2$. *Applied Physics A*, 2006, 83(2): 277-279.
19. Shi Q, Yu X, Feidenhans'l R, et al. Destabilized $LiBH_4$-$NaAlH_4$ Mixtures Doped with Titanium Based Catalysts. *The Journal of Physical Chemistry C*, 2008, 112(46): 18244-18248.
20. Ravnsbæk D B, Jensen T R. Tuning hydrogen storage properties and reactivity: Investigation of the $LiBH_4$-$NaAlH_4$ system. *Journal of Physics and Chemistry of Solids*, 2010, 71(8): 1144-1149.
21. Zhang Y, Tian Q. The reactions in $LiBH_4$-$NaNH_2$ hydrogen storage system. *International Journal of Hydrogen Energy*, 2011, 36(16): 9733-9742.
22. Morelle F, Jepsen L H, Jensen T R, et al. Reaction pathways in $Ca(BH_4)_2$-$NaNH_2$ and $Mg(BH_4)_2$-$NaNH_2$ hydrogen-rich systems. *The Journal of Physical Chemistry C*, 2016, 120(16): 8428-8435.
23. Cho Y W, Shim J H, Lee B J. Thermal destabilization of binary and complex metal hydrides by chemical reaction: A thermodynamic analysis. *Calphad*, 2006, 30(1): 65-69.
24. Kang X D, Wang P, Ma L P, et al. Reversible hydrogen storage in $LiBH_4$ destabilized by milling with Al. *Applied Physics A*, 2007, 89(4): 963-966.
25. Jin S A, Shim J H, Cho Y W, et al. Reversible hydrogen storage in $LiBH_4$-Al-LiH composite powder. *Scripta materialia*, 2008, 58(11): 963-965.
26. Liu H, Wang X, Zhou H, et al. Improved hydrogen desorption properties of $LiBH_4$ by AlH_3 addition. *International Journal of Hydrogen Energy*, 2016, 41(47): 22118-22127.
27. Kwak Y J, Song M Y. How to Analyse Metal Hydride Decomposition Temperatures Using a Sieverts' Type Hydriding-Dehydriding Apparatus and Hydrogen-Storage Characteristics for an MgH_2-Based Alloy. *Materials Science*, 2018, 24(1): 24-28.
28. Züttel A, Rentsch S, Fischer P, et al. Hydrogen storage properties of $LiBH_4$. *Journal of Alloys and Compounds*, 2003, 356: 515-520.
29. Kang X D, Wang P, Ma L P, et al. Reversible hydrogen storage in $LiBH_4$ destabilized by milling with Al. *Applied Physics A*, 2007, 89(4): 963-966.
30. Zhang Y, Tian Q, Zhang J, et al. The dehydrogenation reactions and kinetics of $2LiBH_4$-Al composite. *The Journal of Physical Chemistry C*, 2009, 113(42): 18424-18430.
31. Friedrichs O, Kim J W, Remhof A, et al. The effect of Al on the hydrogen sorption mechanism of $LiBH_4$. *Physical chemistry chemical physics*, 2009, 11(10): 1515-1520.
32. Ravnsbæk D B, Jensen T R. Mechanism for reversible hydrogen storage in $LiBH_4$-Al. *Journal of Applied Physics*, 2012, 111(11): 112621.
33. Hansen B R S, Ravnsbæk D B, Reed D, et al. Hydrogen storage capacity loss in a $LiBH_4$-Al composite. *The Journal of Physical Chemistry C*, 2013, 117(15): 7423-7432.